

## Low thrust inclined circular trajectories for airplanes

Gilles Labonté\*

*Department of Mathematics and Computer Science and Department of Electrical Engineering and Computer Engineering, Royal Military College of Canada, Kingston, Ontario, Canada*

*(Received June 17, 2016, Revised June 28, 2016, Accepted July 8, 2016)*

**Abstract.** Automatic trajectory re-planning is an integral part of unmanned aerial vehicle mission planning. In order to be able to perform this task, it is necessary to dispose of formulas or tables to assess the flyability of various typical flight segments. Notwithstanding their importance, there exist such data only for some particularly simple segments such as rectilinear and circular sub-trajectories. This article presents an analysis of a new, very efficient, way for an airplane to fly on an inclined circular trajectory. When it flies this way, the only thrust required is that which cancels the drag. It is shown that, then, much more inclined trajectories are possible than when they fly at constant speed. The corresponding equations of motion are solved exactly for the position, the speed, the load factor, the bank angle, the lift coefficient and the thrust and power required for the motion. The results obtained apply to both types of airplanes: those with internal combustion engines and propellers, and those with jet engines. Conditions on the trajectory parameters are derived, which guarantee its flyability according to the dynamical properties of a given airplane. An analytical procedure is described that ensures that all these conditions are satisfied, and which can serve for producing tables from which the trajectory flyability can be read. Sample calculations are shown for the Cessna 182, a Silver Fox like unmanned aerial vehicle, and an F-16 jet airplane.

**Keywords:** automatic trajectory planning; airplane circular trajectory; inclined circular trajectories; inclined pendulum trajectories; Dubins 3D trajectories

---

### 1. Introduction

This work is part of a broader study of automatic mission planning for unmanned aerial vehicles (UAVs). Whereas the flight programs of commercial airplanes are normally fairly simple and are specified before the flight takes place, those of UAVs are generally more complex, and very often have to be adapted to unforeseen circumstances during the mission by on-board re-planning the trajectory. For this to be possible, it is necessary to dispose of mathematical formulas or tables that provide information about trajectories that are flyable according to the airplane dynamics, together with other important parameters such as the fuel use and the time of flight. Furthermore, for mission optimization purposes, formulas are required to allow for assigning costs to alternative flyable trajectories. In this article, we present such formulas for a particular type of circular trajectories that lie in inclined planes.

We point out the distinction that can be made between “path planning” and “trajectory

---

\*Corresponding author, Emeritus Professor, E-mail: [gilles.labonte@rmc.ca](mailto:gilles.labonte@rmc.ca)

planning”. In the first process, it is only a “road” that is determined, which airplanes can travel. In the second process, on the other hand, the position and velocity of the airplane on this road are also determined as a function of time. Thus, for mission planning purposes, it is trajectory planning that has to be performed, although path planning would still be a preliminary step.

A preferred approach to automatic path planning involves two stages. In a first stage a stick path is constructed, as a continuous sequence of rectilinear segments. In a second stage, the connections between these segments are smoothed so that the velocity of an airplane on the path would be continuous.

Labonté (2011) and (2015a) analyzed the dynamics of airplanes on rectilinear trajectories, inclined at arbitrary angles, and derived necessary conditions for engine-propeller driven airplanes to be able to fly such trajectories. The formulas obtained allow calculating all the physical parameters involved. We note that the corresponding analysis has not yet been done for jet airplanes, but it would not be difficult to do, with the help of the same method used for propeller airplanes.

There are two main approaches for connecting smoothly the rectilinear segments. The one that is most often used consists in connecting them with arcs of circles, in such a way that the tangent to the path is continuous. This method generalizes to three-dimensional space the well-known two-dimensional paths of Dubins (1957). Thus, these circular arcs may lie in planes at various inclinations with respect to the horizontal. Many authors are concerned only with constructing such paths, without specifying the speed at which they would be flown. This is the case of Anderson (2002), Rathbun *et al.* (2002), Jun and D’Andrea (2003), Torroella (2004), Anderson *et al.* (2005), Jeyaraman *et al.* (2005), Bottasso (2008), Shanmugavel *et al.* (2010), Wang Zhong and Li Yan (2014), Lin and Saripalli (2014), Lugo-Cardenas *et al.* (2014). Some other authors, for reason of simplicity, propose trajectories that correspond to flying these paths at constant speed. This is the case of Chandler *et al.* (2000), Jia and Vagners (2004), Chitsaz and LaValle (2007), Hwangbo *et al.* (2007), Li Xia *et al.* (2009), Ambrosino *et al.* (2009), Babaei and Mortazavi (2010), Hota and Ghose (2010). We note however that none of these authors incorporate the rigorous formulas obtained in Labonté (2011) and (2015a) for the straight segments and those derived in Labonté (2015b) for the inclined circular segments.

Another common path smoothing method employs splines, as described in, among others, Judd (2001), Nikolos *et al.* (2003), Singh and Padhi (2009) and Yang and Sukkarieh (2010). However, this method has the disadvantage of yielding curved connecting curves that are not easily analyzed for their flyability and, to our knowledge, no such analysis of them has yet been performed.

Because they are simpler to analyze, we concentrated our efforts on the circular connections. There are, evidently, infinitely many variable speeds with which these sub-trajectories can be flown. However, at this stage of the study, we look for rather simple speed patterns that correspond to solvable equations of motion, from which appropriate control commands for the airplane can be determined. Even though such solvable systems may appear “oversimplified”, they have great value as a basis for further developments.

It is remarkable that, even for constant speed inclined circular flights, there existed no complete solution until the work of Labonté (2015b). Most airplane dynamics manuals discuss circular trajectories in the horizontal plane, under the heading of “banked turns”. Many also discuss circular trajectories in the the vertical plane as loops, pull-ups or pull-downs. A few have a section on aerobatics where they discuss inverted loops and spiral trajectories (see for example, Chapter 3 of Phillips (2004), Chapter 8 of Mair and Birdsall (1992), and Section 15 of Cowley and Levy (1920)). In all the studies of climbing or descending flights that we found, except when vertical

loops are discussed, the approximation is made that  $\theta_H$ , the angle of the trajectory with the horizontal plane, is small so that  $\cos(\theta_H) \approx 1$ . Although it is true, for many airline airplanes, that  $\theta_H$  is limited to such small values, it is not true for UAVs or high performance fighter airplanes. UAVs come in a wide range of sizes and agilities and they can fly much more daring maneuvers as inhabited airplanes. Thus, in the present study, we do not make the approximation of small inclinations; our analysis covers all angles of inclination.

The present study of low thrust inclined circular trajectories was initiated after Labonté (2015b) clearly showed that the constant speed requirement considerably limits the trajectory inclination. It therefore seemed imperative to find some other analytically manageable way to fly. The one we describe in the present article is relatively simple in nature and involves only familiar mathematical formulas. On such trajectories, the airplane propulsion system only compensates for the aerodynamic drag so that the airplane follows gravity as a simple pendulum would move on an inclined plane. We will solve exactly the equation of motion to yield the position and velocity of the airplane as functions of time. We will derive constraints for the angle of inclination of the trajectories, their radii and the speeds, which correspond to the limits on the load factor, the lift coefficient and the thrust available. We believe that this particular method of flying has not been studied before, and the corresponding equations of motion have not already been solved.

### 1.1 Simplifying assumptions

In his Chapter XVII on “Nonuniform Flight”, Von Mises (1945) states: “the equation of motion for a rigid body with all the six degrees of freedom can be integrated only very seldom”. Furthermore, it would be very complicated to really take into account all the aerodynamic forces acting on the different parts of an airplane in nonuniform motion, because of the asymmetric attitude of the airplane with respect to its trajectory. In this same chapter, Von Mises (1945) discusses vertical loops and banked horizontal turns. In this discussion, he mentions that in curved trajectories, “the air reactions must supply, in addition to the centripetal force ..., a rolling, a pitching, and a yawing moment...” After some calculations, for the banked turn, he comments that, “the moments required for maintaining the steady rotation are unimportant under normal conditions”. Mair and Birdsall (1992) make a similar remark in their Chapter 8 that presents a detailed discussion of vertical loops, horizontal banked turns and helicoidal trajectories. In Section 8.5), they state “that any increase of drag due to the angular velocity of the aircraft and the deflections of the control surfaces can be neglected in comparison with the dominant increase of the lift-dependent drag.” Section 15 of Cowley and Levy (1920) comments similarly that a rigorous treatment of curved flight trajectories would be extremely complicated because of the presence of imperfectly known factors related to the variation in aerodynamic forces along the wings, due to their non-symmetric role in the motion. They assume that “any increase of drag due to the angular velocity of the aircraft and the deflections of the control surfaces can be neglected in comparison with the dominant lift-dependent drag.”

In the present study, we made the same assumptions to the effect that the dynamics involved in the rotations of the airplane about its center of mass are negligible when one is concerned with the motion of its center of mass. We also not take into account the perturbations of the atmosphere. We consider that the circular trajectories are small enough that the air density, the air temperature and the weight of the airplane can be considered constant during the motion. Finally, we make the same remark as that in the introduction to Chapter 3 on “Aircraft Performance” of Phillips (2004) to the effect that the material we present “should be thought of as only a preliminary study of

airplane performance. Here, emphasis is placed on obtaining closed-form analytic solutions suitable for preliminary design.”

### 1.2 Organisation of the article

This article starts with a presentation of the equations of motion for an airplane center of mass on an arbitrary inclined circular trajectory. It then describes a particular type of flight over such trajectories, which is akin to the motion of a pendulum on an inclined plane. The corresponding equations of motion are then solved for the position and speed of the airplane. The required angle of bank is calculated. So is the load factor, and the limits on the trajectory parameters that follow from its bounds are derived. A similar analysis is done to obtain the range of parameters for which the bounds on the lift coefficient are respected. For airplane with propellers, an analysis is made of the upper bound on the power available. For jet airplanes, a similar analysis is concerned with the upper bound on the thrust available.

A procedure is explained that takes into account all the above limits in order to determine the parameters for which inclined circular trajectories are flyable by a given airplane. It is shown how tables of parameters can be constructed to sum up the results obtained. The application of the formulas derived is illustrated with airplanes that have similar properties as the following well known three different airplanes:

- the Cessna 182 Skylane, which has a reciprocating engine with a constant speed propeller,
- a Silver Fox like unmanned aerial vehicle (UAV) which has a reciprocating engine with a fixed pitch propeller,
- the Lockheed-Martin F-16 fighter jet.

We note that these are the same three airplanes that were used in Labonté (2015b), for the sample calculations that determine the flyability of inclined circular trajectories flown at constant speed. This will allow appreciating the improvement in flyability provided by the low thrust motion.

The required characteristics of these airplanes are listed in Appendix A. There may be small differences between the values we use and the actual values for a particular model of these airplanes. We used values that were readily available on the internet and those that were not, were estimated from the values for similar airplanes. This is adequate for our purpose which is to illustrate the calculations involved in the formulas we derive. In all the calculations shown, the load carried by the airplane is taken to be one quarter of its maximum load.

## 2. The equations of motion

We shall use the same formalism for the equations of motion as in Labonté (2015b). We consider an airplane that flies on a circular trajectory that lies in a plane inclined by an angle  $\theta$  with respect to the vertical (or  $\theta_H$  with the horizontal). Such a trajectory is represented in Fig. 1, where we have chosen the coordinate axes so that its horizontal diameter is along the x-axis. We represent by  $\mathbf{n}$  the unit vector that is normal to the plane of the trajectory:

$$\mathbf{n} = [0, -\cos(\theta), \sin(\theta)].$$

The position of the center of mass of the airplane, at time  $t$ , is represented by  $\mathbf{x}(t)$ :

$$\mathbf{x}(t) = \mathbf{C} + R \mathbf{r}$$

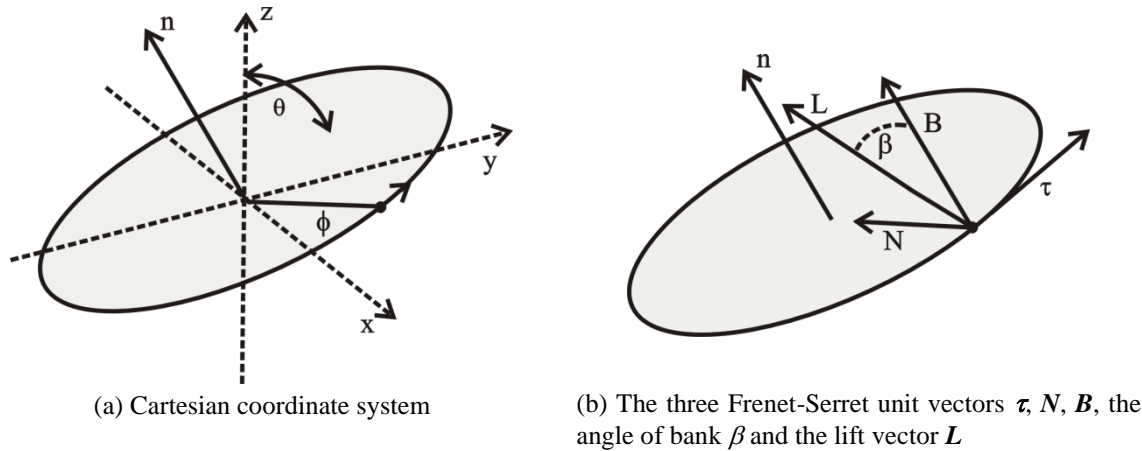


Fig. 1 Parameters used in the description of circular trajectories inclined by an angle  $\theta$  with respect to the vertical

in which

- $\mathbf{r} = [ \cos(\phi), \sin(\theta) \sin(\phi), \cos(\theta) \sin(\phi) ]$  is the unit radial vector
- $\mathbf{C} = [ C_1, C_2, C_3 ]$  is the position of the center of the circle,
- $R$  is its radius,
- $\phi$  is the angle, in the plane of the circular trajectory, which the airplane position vector makes with the x-axis.

If the trajectory is traversed in the counterclockwise direction around the normal  $\mathbf{n}$ ,  $\phi$  is a monotonically increasing function of  $t$ . Otherwise, it is monotonically decreasing. It is such that  $\phi(0)=0$  and  $\phi(P)=2\pi$ , when  $P$  is the period, i.e., the time required to fly around the trajectory. For counterclockwise motion, the airplane is ascending when  $\phi \in [\pi/2, \pi/2]$  and it is descending when  $\phi \in [\pi/2, 3\pi/2]$ . For a constant speed trajectory,  $\phi = \omega t$ , in which  $\omega = 2\pi/P$  is a constant. The airplane velocity is  $\mathbf{v}(t)$ :

$$\mathbf{v}(t) = \mathbf{x}'(t) = V_\infty \boldsymbol{\tau}$$

where

$$V_\infty = R \phi'$$

and

$$\boldsymbol{\tau} = [ -\sin(\phi), \sin(\theta) \cos(\phi), \cos(\theta) \cos(\phi) ].$$

$\boldsymbol{\tau}$  is the unit vector tangent to the trajectory. For constant speed trajectories,  $V_\infty = R\omega$ . For the sake of clarity, we shall hereafter consider that the trajectory is in the counterclockwise direction, so that  $\phi' > 0$  at all times. We shall use the Frenet-Serret frame of reference that is particularly well adapted for the description of such trajectories. Fig. 1(b) shows its basis vectors. The unit principal normal vector  $\mathbf{N}$  is directed toward the center of the circle with  $\mathbf{N} = -\mathbf{r}$ .

The acceleration of the airplane is:  $\mathbf{a}(t) = \mathbf{v}'(t) = R \phi'' \boldsymbol{\tau} + \frac{V_\infty^2}{R} \mathbf{N}$ . The unit binormal vector  $\mathbf{B}$  is simply the vector  $\mathbf{n}$ .

### 2.1 The forces involved

The physical forces at play are

- the lift  $\mathbf{L}$ ,
- the gravitational force  $\mathbf{W} = -W\mathbf{k}$ , with  $\mathbf{k} = [0, 0, 1]$ ,
- the longitudinal force that corresponds to the thrust produced by the propulsion system  $T$  minus the drag  $D$ ; its value is then  $(T-D)\boldsymbol{\tau}$ .

The lift  $\mathbf{L}$  is perpendicular to the velocity of the airplane. The bank angle  $\beta$ , is measured with respect to the normal to the plane of the trajectory,  $\mathbf{L}$  can be written as:

$$\mathbf{L} = L \cos(\beta) \mathbf{n} + L \sin(\beta) \mathbf{N}(t)$$

Fig. 1(a) shows how the bank angle is defined; it can take any value, corresponding to the airplane flying in any possible attitude on the trajectory. Newton's equation of motion is:

$$\frac{W}{g} \mathbf{a} = \mathbf{L} + \mathbf{W} + (T-D) \boldsymbol{\tau} \quad (1)$$

The  $\mathbf{n}$ ,  $\mathbf{N}$  and  $\boldsymbol{\tau}$  components of this equation are respectively

$$L \cos(\beta) = W \sin(\theta) \quad (2)$$

$$L \sin(\beta) = \frac{WV_{\infty}^2}{gR} - W \cos(\theta) \sin(\phi), \quad (3)$$

$$T = D + \frac{WR}{g} \phi'' + W \cos(\theta) \cos(\phi) \quad (4)$$

We define  $A_c$ , the centripetal acceleration in units of  $g$  as

$$A_c = \frac{V_{\infty}^2}{gR} - \cos(\theta) \sin(\phi). \quad (5)$$

Eq. (3) can then be written as

$$L \sin(\beta) = W A_c. \quad (6)$$

We note that, for non-vertical trajectories, the lift  $L$  cannot change sign on the trajectory, since then there would have to be a position  $\phi$  at which  $L=0$ , but this cannot happen since the RHS of Eq. (2) is a positive constant. The same argument holds for  $\cos(\beta)$ . Thus,  $L$  and  $\cos(\beta)$  must keep the same sign, either positive or negative, at every point of the trajectory, and this sign has to be the same one for both of them. In particular, this means that the lift coefficient  $C_L$  must keep the same sign on the whole trajectory.

We further note that in the upper section of the trajectory, i.e., when  $\phi \in (0, \pi)$ , the gravitational force acting on the airplane has a component toward the center of the trajectory. As can be seen in Eq. (3), this force cancels part of the centrifugal force. It may actually happen that, near the top of the trajectory about  $\phi = \pi/2$ , this force is stronger than the centrifugal force. In that case, it will be necessary for the angle of bank to be negative in this region, in order for the lift to prevent the airplane from falling toward the center of the circle.

### 3. Low thrust trajectories

When considering Eq. (4) for the thrust required, one can see that if the last two terms cancelled out, then the only thrust required would be that to cancel the drag, since then  $T=D$ . In that sense, this way of flying could be considered optimal in terms of thrust or power requirements. An advantage of such trajectories is that the requirement for positivity of the thrust does not impose constraints on the trajectory parameters, as was the case for those flown at constant speed, as shown in Labonté (2015b).

For such trajectories, the angle  $\phi$  changes in time according to the following equation

$$\phi'' + \frac{g}{R} \cos(\theta) \cos(\phi) = 0 \tag{7}$$

Note that for horizontal trajectories,  $\theta=\pi/2$ ; Eq. (7) then reduces to  $\phi'=0$ . This implies that  $\phi'=constant$  and thus that the speed  $V_\infty$  is constant. It is noteworthy that for inclined trajectories, the rate of change of  $\phi$  is the same as for the angle of suspension of a pendulum that lies on the plane, inclined at the angle  $\theta$ . Correspondingly, the solution to Eq. (7) can be found in many textbooks on Classical Mechanics, such as in ‘‘Section 5.4 The Plane Pendulum’’ of Marion (1970). When Eq. (7) is multiplied by  $R^2 \phi'$ , one obtains an equation that is readily integrated to yield

$$\frac{1}{2} V_\infty^2 + g Z [1 + \sin(\phi)] = E \tag{8}$$

in which we have defined the constant  $Z$ :  $Z=R\cos(\theta)$ , which is the altitude of the highest point of the trajectory, and in which  $E$  is a positive constant of integration. For a simple pendulum,  $E$  would be the total energy divided by the mass. When  $\phi=-\pi/2$ , i.e., at the bottom of the trajectory,  $E = \frac{1}{2} V_\infty^2$  and when  $\phi=\pi/2$ , i.e., at the top,  $E = \frac{1}{2} V_\infty^2 + 2gZ$ . According to Eq. (8), the minimum and maximum values of the speed,  $V_m$  and  $V_M$  are respectively such that:

$$V_m^2 = 2 \{ E - 2gZ \} \text{ at } \phi = \pi/2$$

and

$$V_M^2 = 2E \text{ at } \phi = -\pi/2. \tag{9}$$

For the airplane to travel the whole circular trajectory, we require that the speed be positive at all times so that it is required that

$$E > 2gZ. \tag{10}$$

According to Eqs. (8) and (5),

$$A_c = \frac{1}{gR} \left[ \frac{3V_\infty^2}{2} - E + gZ \right]. \tag{11}$$

#### 3.1 Solution to the equations of motion

Upon using the expression for  $V_\infty$  given in Eq. (2.5) and solving Eq. (8) for  $\phi'$ , one obtains

$$\frac{d\phi}{\sqrt{E - gZ[1 + \sin(\phi)]}} = \frac{\sqrt{2}}{R} dt. \quad (12)$$

If we let the airplane be at the bottom of the trajectory, where  $\phi = -\pi/2$ , at  $t=0$ , then the integration of Eq. (12) yields

$$\int_{-\pi/2}^{\phi} \frac{d\psi}{\sqrt{E - gZ[1 + \sin(\psi)]}} = \frac{\sqrt{2}}{R} t. \quad (13)$$

The change of variable:  $x = \psi/2 + \pi/4$  transforms Eq. (13) into

$$\int_0^{\phi/2 + \pi/4} \frac{dx}{\sqrt{1 - k^2 \sin^2(x)}} = \lambda t \quad (14)$$

in which

$$\lambda = \frac{\sqrt{E}}{R\sqrt{2}}$$

and

$$k = \sqrt{\frac{2gZ}{E}}. \quad (15)$$

Note that  $k < 1$  by virtue of Ineq. (10), which reflects the fact that the total energy should be larger than the maximum potential energy on the trajectory of the analogous pendulum. The value of the integral can be found in mathematical tables such as that of Gradshteyn and Ryzhik (1965), Section 8.111 and 8.14. Eq. (14) is seen to yield

$$F\left(\frac{\phi}{2} + \frac{\pi}{4}, k\right) = \lambda t, \quad (16)$$

where  $F$  is the Jacobi elliptic integral of the first kind. The airplane finishes a complete circle when  $\phi = 3\pi/2$ ; which occurs at the time  $t_{3\pi/2}$  such that

$$t_{3\pi/2} = \frac{1}{\lambda} F(\pi, k). \quad (17)$$

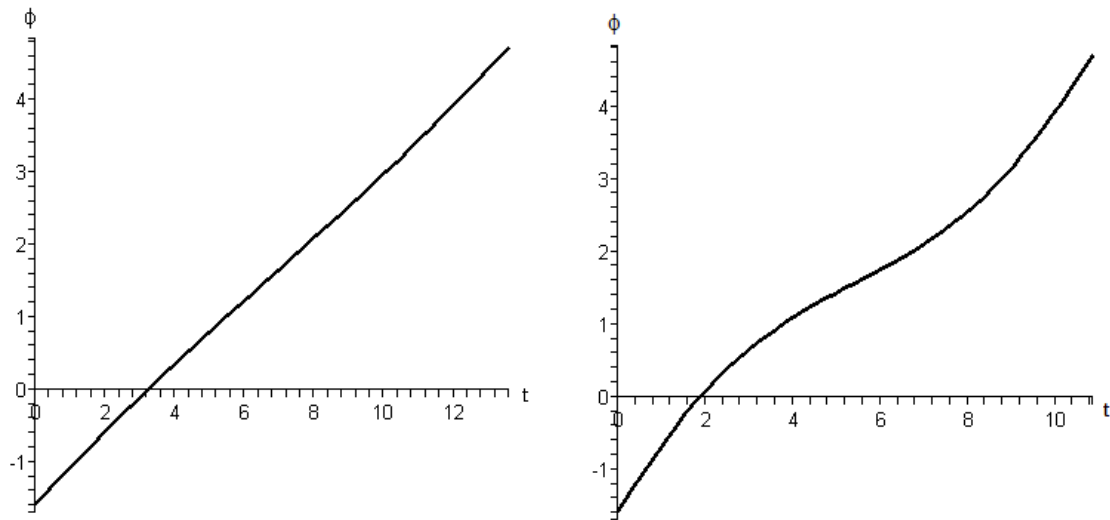
The function  $F$  has an inverse, called the Jacobi amplitude, which is denoted by “am”, so that if  $u = F(\phi, k)$ , then

$$\phi = F^{-1}(u, k) = \text{am}(u, k). \quad (18)$$

Thus, Eq. (16) implies

$$\phi = 2 \text{am}(\lambda t, k) - \frac{\pi}{2}. \quad (19)$$

Fig. 2(a) shows the position angle  $\phi$  as a function of time  $t$ , for the Cessna 182 on a trajectory



(a) Cessna 182 with  $\theta_H=10^\circ$ ,  $R=100$  m,  $E=1250$  m<sup>2</sup>/s<sup>2</sup> (b) Silver Fox with  $\theta_H=50^\circ$ ,  $R=40$  m,  $E=680$  m<sup>2</sup>/s<sup>2</sup>

Fig. 2 Angle of rotation  $\phi$  as a function of time

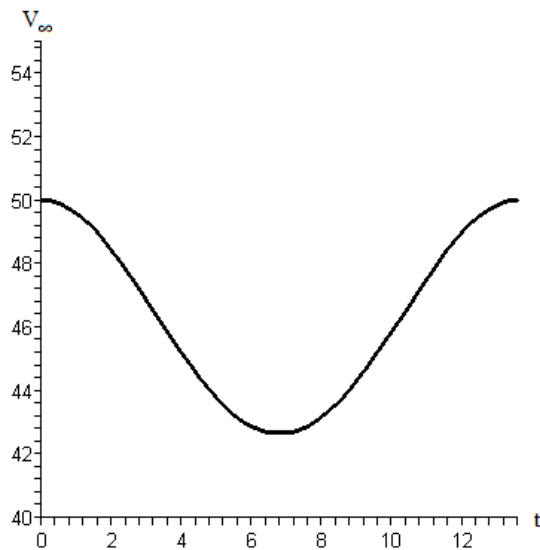


Fig. 3 Speed  $V_\infty$  as a function of time for the Cessna 182 on the trajectory with  $\theta_H=10^\circ$ ,  $R=100$  m and  $E=1250$  m<sup>2</sup>/s<sup>2</sup>

inclined with respect to the horizontal plane at an angle of  $\theta_H=10^\circ$ , with radius  $R=100$  m and  $E=1250$  m<sup>2</sup>/s<sup>2</sup>. One can see that, in that case,  $\theta_H$  is small enough for  $\phi$  to vary almost linearly with  $t$ . Fig. 2(b) shows  $\phi(t)$  for the Silver Fox, on a trajectory inclined at of  $\theta_H=50^\circ$ , with  $R=40$  m and  $E=680$  m<sup>2</sup>/s<sup>2</sup>. At such an inclination, the non-linearity of  $\phi(t)$  is more apparent.

Fig. 3 shows the graph of  $V_\infty$  as a function of time for the Cessna 182 on the trajectory mentioned above.

## 4. Bank angle

### 4.1 Vertical loops

In a vertical loop,  $\theta=0$  and Eq. (2) then implies that  $\cos(\beta)=0$  so that the bank angle  $\beta$  is either  $\pi/2$  or  $-\pi/2$  everywhere on the trajectory. The first case corresponds to the loop that is usually performed in aerobatics shows, in which the airplane is upside up at the bottom of the loop and upside down at the top. The case with the angle of bank  $\beta=-\pi/2$ , corresponds to an inverted loop in which the airplane is upside down at the bottom of the loop and upside up at the top.

### 4.2 Non-vertical loops

When  $\theta \neq 0$ , we divide Eq. (6) by Eq. (2) and obtain the following equation for the bank angle

$$\tan(\beta) = \frac{A_c}{\sin(\theta)}. \quad (20)$$

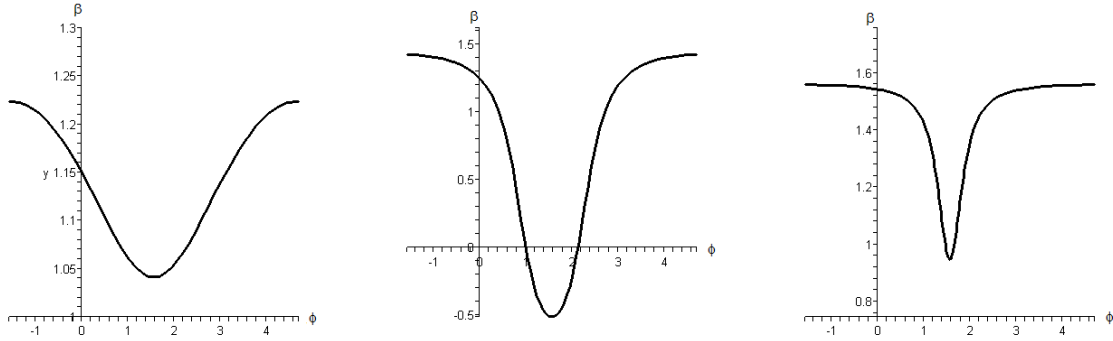
This equation indicates that all airplanes must bank by the same angle  $\beta$  in order to travel with the same speed  $V_\infty$  on this circular trajectory, as well as for vertical loops, a fact that generalizes a well-known property of horizontal circular trajectories, see for example in Chapter 2 of Stengel (2004). From Eq. (20), it follows that

$$\begin{aligned} \sin(\beta) &= \varepsilon \frac{A_c}{\sqrt{\sin^2(\theta) + A_c^2}} \\ \cos(\beta) &= \varepsilon \frac{\sin(\theta)}{\sqrt{\sin^2(\theta) + A_c^2}} \end{aligned} \quad (21)$$

with  $\varepsilon=\pm 1$ . If the airplane is flying upside up at the bottom of the trajectory, where  $A_c$  is positive, then  $\beta \in [0, \pi/2]$  at this point so that  $\varepsilon=+1$ . The lift vector points toward the region above the circular trajectory. In that case  $\cos(\beta)>0$  on the whole trajectory. If the trajectory parameters are such that  $2E-5gR\cos(\theta)<0$ , then  $A_c$  will be negative in the interval  $(\phi_0, \pi-\phi_0)$ , centered on  $\pi/2$ , where  $\phi_0$  and  $\pi-\phi_0$  are the angles at which  $A_c=0$ . In this region  $\sin(\beta)<0$  so that  $\beta<0$  and the lift vector points away from the region above the circular trajectory. How the bank then varies can be seen in the middle of Fig. 4. In the situation in which the airplane is flying upside down at the bottom of the trajectory, then  $\varepsilon=-1$ , and the above described situation prevails with the opposite sign everywhere for the bank angle  $\beta$ . The bank angle is symmetric by reflection through the angle  $\pi/2$  and through the angle  $-\pi/2$  (or  $3\pi/2$ ). Its minimum value occurs at  $\phi=\pi/2$  and its maximum value is at  $\phi=-\pi/2$  (or  $3\pi/2$ ).

We note that, as mentioned in our introduction, we have not taken into account the dynamic constraints ruling the rolling motion of the airplane. However, it could happen that the change in the bank angle requires the roll to be rapid, as can be seen on the RHS of Fig. 4. In such a situation, it may then happen that the force required to move the ailerons or the stress on the airframe would be too large for that motion to be possible. A simple way of taking this situation into account would be to impose a limit on the rate of variation of  $\beta$  with respect to  $\phi$ , such as

$\left| \frac{\partial \beta}{\partial \phi} \right| \leq \text{some constant}$ . We have not implemented such a bound in the present exploratory study.



(a) Cessna 182 with  $\theta_H=10^\circ$ ,  $R=100$  m,  $E=1250$  m<sup>2</sup>/s<sup>2</sup>    (b) Silver Fox with  $\theta_H=50^\circ$ ,  $R=40$  m,  $E=680$  m<sup>2</sup>/s<sup>2</sup>    (c) F16 with  $\theta_H=85^\circ$ ,  $R=400$  m,  $E=10\,000$  m<sup>2</sup>/s<sup>2</sup>

Fig. 4 Graph of the bank angle  $\beta$  as functions of  $\phi$  that varies from  $-\pi/2$  to  $3\pi/2$

Fig. 4(a) shows how the bank angle  $\beta$  varies as  $\phi$  varies from  $-\pi/2$  to  $3\pi/2$  for the Cessna 182 on a circular trajectory inclined with  $\theta_H=10^\circ$ ,  $R=100$  m and  $E=1250$  m<sup>2</sup>/s<sup>2</sup>. Fig. 4(b) shows the corresponding curve for the Silver Fox when  $\theta_H=50^\circ$ , with  $R=40$  m and  $E=680$  m<sup>2</sup>/s<sup>2</sup>. In that case,  $A_c$  and thus  $\beta$  are negative when  $\phi \in (1.00, 2.14)$ . Fig. 4(c) shows the bank angle for the F-16 on a trajectory with  $\theta_H=85^\circ$ ,  $R=400$  m and  $E=10\,000$  m<sup>2</sup>/s<sup>2</sup>.

### 5. Load factor

For vertical loops, in which  $\theta=0$ , Eq. (6) gives the load factor as

$$n = \frac{L}{W} = \varepsilon A_c . \tag{22}$$

In a right-side-up loop, if the parameters are such that  $A_c$  becomes negative for certain angles  $\phi$  about  $\pi/2$ , i.e., at the top of the loop, then the load factor will be negative at these positions.

For non-vertical loops, as discussed after Eq. (6), the load factor keeps the same sign on the whole trajectory. According to Eq. (2) the load factor is

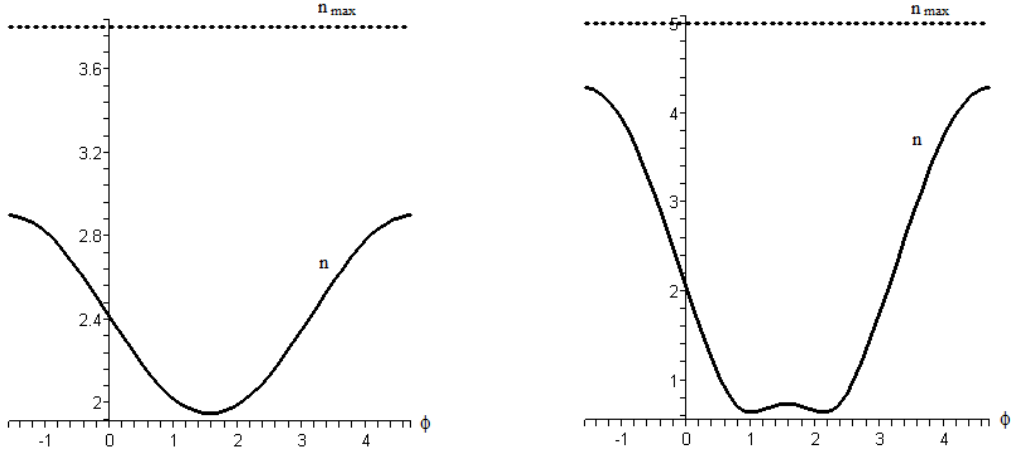
$$n = \frac{L}{W} = \varepsilon \sqrt{\sin^2(\theta) + A_c^2} , \tag{23}$$

with  $\varepsilon = \pm 1$  as in Eq. (21), and, as is the case for  $L$ , the load factor keeps the same sign on the whole trajectory, which is the same one as the bank angle. The structural integrity of the airplane requires that the load factor  $n$  be bounded such that

$$n_{min} \leq n \leq n_{max} . \tag{24}$$

Thus, from Eqs. (11), (23) and (24), one can deduce that

$$\left[ \frac{3}{2} V_\infty^2 - E + gZ \right]^2 \leq g^2 R^2 \left[ n_{lim}^2 - \sin^2(\theta) \right], \text{ with } n_{lim} = \begin{cases} n_{max} & \text{if } \varepsilon = +1 \\ n_{min} & \text{if } \varepsilon = -1 \end{cases} . \tag{25}$$



(a) Cessna 182 with  $\theta_H=10^\circ$ ,  $R=100$  m,  $E=1250$  m<sup>2</sup>/s<sup>2</sup> (b) Silver Fox with  $\theta_H=50^\circ$ ,  $R=40$  m,  $E=680$  m<sup>2</sup>/s<sup>2</sup>

Fig. 5 Graph of the load factor  $n$  as a function of the position angle  $\phi$ , together with  $n_{\max}$

Again, for the sake of clarity, we shall hereafter consider trajectories on which  $\varepsilon=+1$ ; the case with  $\varepsilon=-1$  can be dealt with in the same way. We note that Ineq. (25) hold  $\forall V_\infty$  if and only if it holds when its LHS is maximum. After a brief study of this LHS one can determine that this occurs at  $V_\infty=V_m$ . Upon evaluating Ineq. (25) at this point, one obtains

$$E \leq \frac{g}{2} \left\{ -Z + R \sqrt{n_{\max}^2 - \sin^2(\theta)} \right\}. \quad (26)$$

Because of Ineq. (10), when Ineq. (26) holds, it is required that

$$\cos(\theta) < \sqrt{\frac{n_{\max}^2 - 1}{24}} \quad (27)$$

Fig. 5(a) shows how the load factor varies as a function of the angle  $\phi$  along the trajectory, for the Cessna 182 on a circular trajectory inclined with  $\theta_H=10^\circ$ ,  $R=100$  m and  $E=1250$  m<sup>2</sup>/s<sup>2</sup>. The maximum allowed value  $n_{\max}$  is also shown on the graph. As can be seen, Ineq. (24) is satisfied in this situation. Fig. 5(b) shows the corresponding curve for the Silver Fox, when  $\theta_H=50^\circ$  and  $R=40$  m and  $E=680$  m<sup>2</sup>/s<sup>2</sup>.

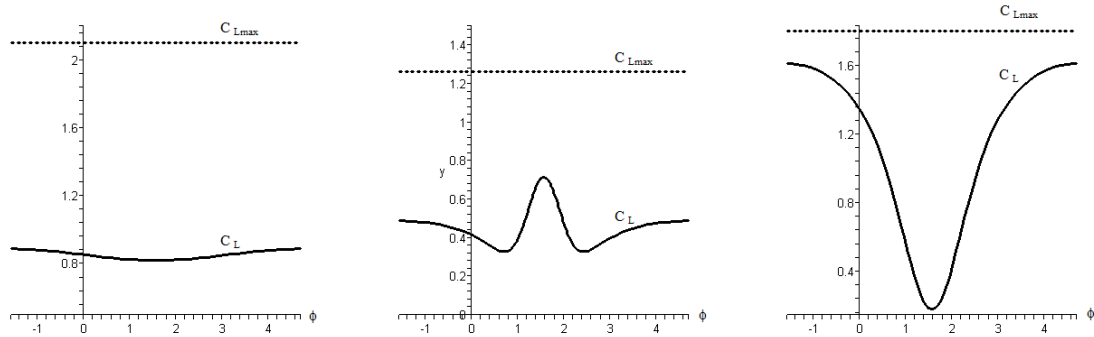
## 6. Lift coefficient

The lift coefficient has to be bounded as follows

$$C_{Lmin} \leq C_L \leq C_{Lmax}. \quad (28)$$

Upon replacing  $L$  in Eq. (6) by its expression, and using Eqs. (21) and (11), one obtains

$$C_L^2 = \left\{ \frac{2W}{g R \rho_\infty S V_\infty^2} \right\}^2 \left\{ g^2 R^2 \sin^2(\theta) + \left[ \frac{3V_\infty^2}{2} - E + gZ \right]^2 \right\}. \quad (29)$$



(a) Cessna 182 with  $\theta_H=10^\circ$ ,  $R=100$  m,  $E=1250$  m<sup>2</sup>/s<sup>2</sup>    (b) Silver Fox with  $\theta_H=50^\circ$ ,  $R=40$  m,  $E=680$  m<sup>2</sup>/s<sup>2</sup>    (c) F16 with  $\theta_H=85^\circ$ ,  $R=400$  m,  $E=10\,000$  m<sup>2</sup>/s<sup>2</sup>

Fig. 6 Graph of the lift coefficient  $C_L$  as a function of the angle  $\phi$ , together with  $C_{Lmax}$

Fig. 6(a) shows how the lift coefficient  $C_L$  varies as a function of the angle  $\phi$  along the trajectory, for the Cessna 182 on a circular trajectory inclined with  $\theta_H=10^\circ$ ,  $R=100$  m and  $E=1250$  m<sup>2</sup>/s<sup>2</sup>. The maximum allowed value  $C_{Lmax}$  is also shown on the graph. Fig. 6(b) shows the corresponding curve, for the Silver Fox, on a trajectory inclined at of  $\theta_H=50^\circ$ , with  $R=40$  m and  $E=680$  m<sup>2</sup>/s<sup>2</sup>. Fig. 6(c) shows the corresponding graph for the F-16 on a trajectory inclined with  $\theta_H=85^\circ$ ,  $R=400$  m and  $E=10\,000$  m<sup>2</sup>/s<sup>2</sup>.

For flights in which the airplane is flying upside up, Ineq. (28) requires that  $C_L \leq C_{Lmax}$ . Upon squaring each of its sides and expanding  $C_L$ , this inequality can be written as

$$F(V_\infty^2) \leq 0$$

with

$$F(U) = \alpha U^2 - 3[E - gZ]U + A \tag{30}$$

in which

$$\alpha = \frac{9}{4} - KC_{Lmax}^2, \quad K = \left[ \frac{g R \rho_\infty S}{2W} \right]^2 \quad \text{and} \quad A = E^2 - 2EgZ + g^2R^2. \tag{31}$$

Note that Ineq. (30) holds if and only if it holds at the maximum value of  $F$ .

If  $\alpha=0$ , the function  $F$  corresponds to a straight line with a negative slope. It is then maximum at  $V_m^2$  and Ineq. (30) is therefore satisfied if and only if it holds for  $V_m^2$ .

If  $\alpha \neq 0$ , the function  $F$  corresponds to a parabola, with summit at  $U_s$ :

$$U_s = \frac{3[E - gZ]}{2\alpha}.$$

If  $\alpha < 0$ , the parabola is concave downward and its maximum occurs at a point on the negative  $U$ -axis. It is therefore decreasing along the positive  $U$ -axis, and its maximum value again occurs at  $V_m^2$ , so that Ineq. (30) will be satisfied if and only if it holds at that point.

If  $\alpha > 0$ , the parabola is concave upward and its minimum is on the positive  $U$ -axis.  $F$  is maximum at either  $V_m^2$  or  $V_M^2$ .

Therefore, in all cases, Ineq. (30) will hold if and only if it holds at both  $V_m^2$  and  $V_M^2$ . This condition requires that

$$(4\alpha - 5)E^2 + 4gZE + g^2R^2 \leq 0 \quad (32)$$

and

$$(4\alpha - 5)E^2 + 16(1 - \alpha)gZE + [4(4\alpha - 3)g^2Z^2 + g^2R^2] \leq 0. \quad (33)$$

Clearly,  $(4\alpha - 5)$  has to be negative, otherwise the left-hand-side (LHS) of Ineq. (32) would always be positive. This condition on  $\alpha$  implies that

$$R > \frac{2W}{g \rho_\infty S C_{Lmax}}. \quad (34)$$

The two expressions on the LHS of Ineqs. (32) and (33) then correspond to downward concave parabolas. The maximum of the parabola corresponding to the LHS of Ineq. (32) is on the positive axis, and its intercept on the vertical axis is positive. Therefore, Ineq. (32) will be satisfied when  $E$  larger or equal to the largest root of the LHS, that is

$$E \geq \frac{g}{(5 - 4\alpha)} \left\{ 2Z + \sqrt{4Z^2 + (5 - 4\alpha)R^2} \right\}. \quad (35)$$

The maximum of the parabola that corresponds to the LHS of Ineq. (33) has its maximum at

$$E_c = \frac{8(1 - \alpha)gZ}{(5 - 4\alpha)}.$$

But because of Ineq. (10),  $E > E_c$  so that Ineq. (33) is satisfied if and only if and only if  $E \geq$  the largest root of the LHS, that is

$$E \geq \frac{g}{(5 - 4\alpha)} \left\{ 8(1 - \alpha)Z + \sqrt{4Z^2 + (5 - 4\alpha)R^2} \right\}. \quad (36)$$

## 7. Power for propeller airplanes

### 7.1 Power available

The power available with an engine-propeller propulsion system is bounded above, thus a given trajectory will be possible only if the power required by the airplane to travel this trajectory  $P_R$  always remains below the maximum power available  $P_{Amax}$ . Therefore, the inequality  $P_R \leq P_{Amax}$  must hold at all points of the trajectory. For airplanes with propellers, the power available  $P_A$  is given by

$$P_A = \eta(J)P, \quad (37)$$

in which  $\eta$  is the propeller efficiency and  $P$  is the brake power produced by the engine.  $\eta$  generally

depends on the advance ratio  $J$ , which is defined as

$$J = \frac{V_\infty}{n_p D_p} . \quad (38)$$

$n_p$  is the number of revolution per second that the propeller makes and  $D_p$  is its diameter. Thus the maximum power available  $P_{Amax}$  will be

$$P_{Amax} = \eta(J)P_{max} \quad (39)$$

in which  $P_{max}$  is the maximum power the engine can produce.

Some methods have been proposed to determine  $\eta$  theoretically; see, for example, the survey in Korkan *et al.* (1980). However, these authors mention the difficulties of constructing accurate models. They compared theoretical predictions of various models with experimental data and found that some of the theoretical models produce good results, but many have relatively large discrepancies in some range of  $J$ . In all of these analyses, the algebraic expressions for  $\eta$  would be too complex to allow for an analytical treatment of the power sufficiency condition. Thus, not being able to obtain a general solution to the inequalities involved, we propose an analysis procedure based solely on the possibility of computing the value of  $\eta$  whatever the method used. In particular, this procedure would be straightforward to apply if the values of  $\eta$  were obtained experimentally and then  $\eta$  were represented by a spline.

### 7.2 Power required

Upon multiplying Eq. (4) by the speed  $V_\infty$ , one obtains the following expression for the power  $P_R$  that the airplane power plant must provide for the airplane to follow this trajectory

$$P_R = V_\infty D = \frac{1}{2} \rho_\infty S C_D V_\infty^3 = \frac{1}{2} \rho_\infty S \left[ C_{D0} + \frac{C_L^2}{\pi e AR} \right] V_\infty^3 . \quad (40)$$

When  $C_L$  is replaced by its value from Eq. (29), one obtains

$$P_R = \bar{C}_{D0} V_\infty^3 + \frac{\Gamma}{V_\infty} \left\{ g^2 R^2 \sin^2(\theta) + \left[ \frac{3V_\infty^2}{2} - E + gZ \right]^2 \right\} \quad (41)$$

in which

$$\bar{C}_{D0} = \frac{1}{2} \rho_\infty S C_{D0} ,$$

$$\Gamma = \frac{\gamma}{g^2 R^2}$$

and

$$\gamma = \frac{2W^2}{\pi e AR \rho_\infty S} . \quad (42)$$

Upon rearranging its terms,  $P_R$  can be written in a somewhat simplified form as

$$P_R = CV_\infty^3 - 3\Gamma[E - gZ]V_\infty + \Gamma AV_\infty^{-1}$$

with

$$C = \bar{C}_{D0} + \frac{9}{4}\Gamma, \quad (43)$$

and  $A$  is the same variable as defined in Eq. (31). Some important characteristics of the power required  $P_R$  as a function of  $V_\infty$  are readily obtained by computing its first and second derivatives. Its first derivative is

$$\frac{dP_R}{dV_\infty} = V_\infty^{-2} Q(V_\infty)$$

with

$$Q(V_\infty) = 3CV_\infty^4 - 3\Gamma[E - gZ]V_\infty^2 - \Gamma A. \quad (44)$$

There are two values of  $V_\infty^2$  at which this derivative is null, which are the two roots of  $Q$ . Only one of these is positive at  $V_\infty = V_c$  with

$$V_c^2 = \frac{1}{6C} \left[ 3\Gamma[E - gZ] + \sqrt{9\Gamma^2[E - gZ]^2 + 12\Gamma AC} \right]. \quad (45)$$

The second derivative of  $P_R$  is

$$\frac{d^2 P_R}{dV_\infty^2} = 2\Gamma AV_\infty^{-3} + 6CV_\infty. \quad (46)$$

It is positive everywhere so that  $P_R$  is a function that is concave upward everywhere with a single minimum at  $V_c$ . The RHS of Fig. 8 shows the maximum power available  $P_{Amax}$  and the

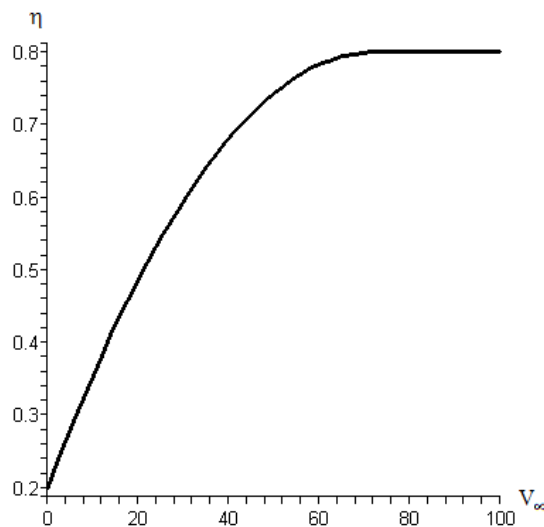


Fig. 7 Efficiency factor  $\eta$  as a function of the speed  $V_\infty$  for the Cessna 182

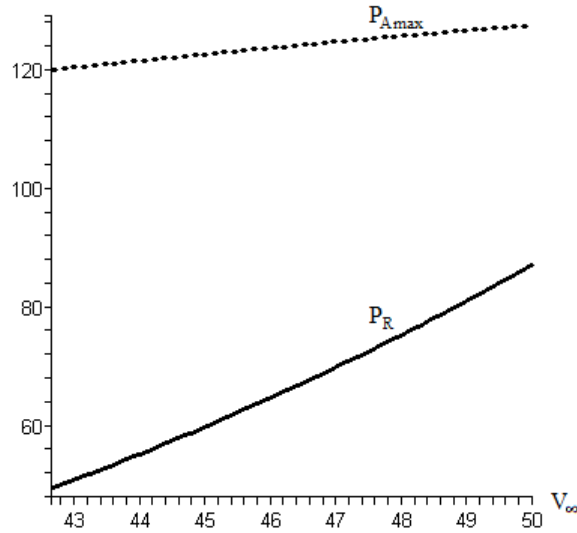


Fig. 8 Maximum power available  $P_{Amax}$  and power required  $P_R$ , as functions of the speed  $V_\infty$ , for the Cessna 182, on a trajectory with  $\theta_H=10^\circ$ ,  $R=100$  m,  $E=1250$  m<sup>2</sup>/s<sup>2</sup>.  $P_R$  and  $P_{Amax}$  have been divided by 1000

power required  $P_R$ , as functions of the speed  $V_\infty$  for the Cessna 182 on a circular trajectory inclined with  $\theta_H=10^\circ$ ,  $R=100$  m and  $E=1250$  m<sup>2</sup>/s<sup>2</sup>.

### 7.3 Upper bound on $P_R$ for airplanes with constant speed propellers

We use the Cessna 182 Skylane as representative of airplanes with a constant speed propeller. The efficiency of its propeller, as a function of the speed  $V_\infty$ , has the general features shown in Fig. 7. This figure has been produced by approximating the curve given in Cavcar (2004) by the following quadratics

$$\begin{aligned} \eta(J) &= -1.036 [J - 0.8]^2 + 0.8 \\ &\forall J \leq 0.8. \\ \eta(J) &= 0.8 \\ &\forall J > 0.8. \end{aligned} \tag{47}$$

Fig. 8 shows both the maximum power available  $P_{Amax}$  and the power required  $P_R$ , as functions of the speed  $V_\infty$ , for a trajectory with  $\theta_H=10^\circ$ ,  $R=100$  m and  $E=1250$  m<sup>2</sup>/s<sup>2</sup>. Note that both  $P_R$  and  $P_{Amax}$  have been divided by 1000. As can be seen in this figure, the Cessna 182 can follow the circular trajectory considered because the power it requires is smaller than the power that its propulsion system can provide.

### 7.4 Upper bound on $P_R$ for airplanes with fixed pitch propellers

We use the Silver Fox like UAV to illustrate the calculations for airplanes with fixed pitch propellers. The efficiency of its propeller  $\eta$ , as a function of  $V_\infty$ , has the general features shown in

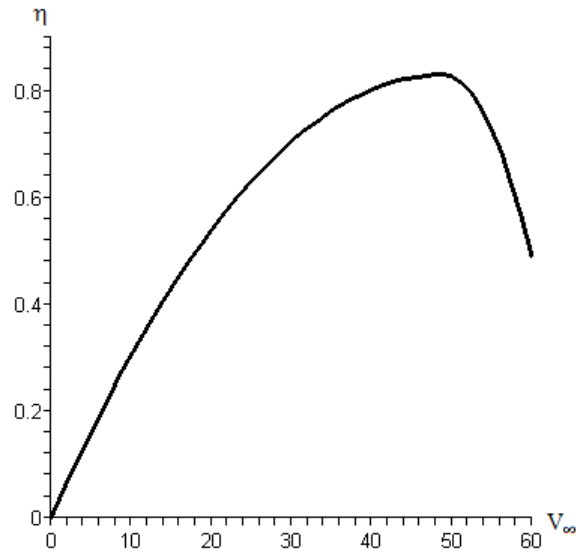


Fig. 9 Efficiency factor  $\eta$  as a function of the speed  $V_\infty$ , for the Silver Fox

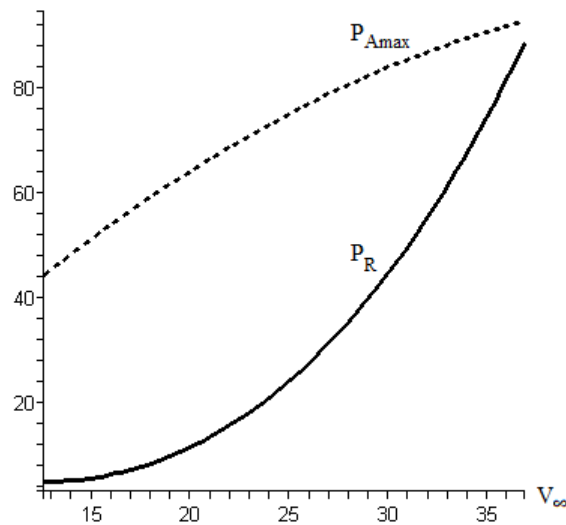


Fig. 10 Maximum power available  $P_{Amax}$  and power required  $P_R$ , as functions of the speed  $V_\infty$  for the Silver Fox on a circular trajectory inclined with  $\theta_H=50^\circ$ ,  $R=40$  m,  $E=680$  m<sup>2</sup>/s<sup>2</sup>. Both  $P_R$  and  $P_{Amax}$  have been divided by 10

Fig. 9. This figure has been produced by approximating with quadratics the curve given in the Aeronautics Learning Laboratory for Science Technology and Research (ALLSTAR) of the Florida International University (2011). Thus, we consider

$$\eta(J) = -1.694[J - 0.70]^2 + 0.83$$

$$\forall J \leq 0.7$$

$$\eta(J) = -13.833 [J - 0.70]^2 + 0.83$$

$$\forall J > 0.7. \tag{48}$$

Fig. 10 shows both the maximum power available  $P_{Amax}$  and the power required  $P_R$ , as functions of the speed  $V_\infty$  for the Silver Fox on a circular trajectory inclined with  $\theta_H=50^\circ$ ,  $R=40$  m and  $E=680$  m<sup>2</sup>/s<sup>2</sup>. Both  $P_R$  and  $P_{Amax}$  have been divided by 10. As this graph shows, the Silver Fox like UAV has enough power to follow the circular trajectory considered because the power it requires is lower than the power its engine-propeller system can provide.

### 7.5 Testing for power sufficiency

We have proven in Section 8.1 that the power required for the circular trajectories is a function of  $V_\infty$  that is concave upward. On the other hand, the curve of maximum power available for airplanes with propellers is concave downward. These facts imply that if and only if the constraint  $P_R \leq P_{Amax}$  holds for  $V_m$  and for  $V_M$ , it will hold for all other  $V_\infty$  along the trajectory.

At  $V_M$ ,  $P_R$  can be written in terms of  $E$  as

$$P_R(V_M) = (2E)^{-1/2} \{ 4(\bar{C}_{D0} + \Gamma)E^2 + 2\Gamma g Z E + \Gamma g^2 R^2 \} \tag{49}$$

with

$$\frac{dP_R(V_M)}{dE} = (2E)^{-3/2} \{ 12(\bar{C}_{D0} + \Gamma)E^2 + 4\Gamma g Z E - \Gamma g^2 R^2 \}.$$

The second derivative of  $P_R(V_M)$  is positive everywhere, and thus it is an upward concave function of  $E$ . Since its first derivative has a zero on the positive  $E$ -axis, it has a minimum at this point. It may then meet  $P_{Amax}(V_M)$  at most at two values of  $E$ , with  $P_R(V_M) \leq P_{Amax}(V_M)$  for all  $E$  between these two values. Fig. 11(a) shows the curves of  $P_R(V_M)$  and  $P_A(V_M)$  as a function of  $E$  for the Cessna 182. This graph indicates that  $P_R(V_M) \leq P_{Amax}(V_M)$  is satisfied for all values of  $E$  between 500 and 1700 m<sup>2</sup>/s<sup>2</sup>.

At  $V_m$ ,  $P_R$  can be written in terms of  $E$  as

$$P_R(V_m) = (2Y)^{-1/2} \{ 4(\bar{C}_{D0} + \Gamma)Y^2 - 2\Gamma g Z Y + \Gamma g^2 R^2 \} \text{ with } Y = E - 2gZ$$

$$\frac{dP_R(V_m)}{dY} = (2Y)^{-3/2} \{ 12(\bar{C}_{D0} + \Gamma)Y^2 - 4\Gamma g Z Y - \Gamma g^2 R^2 \}. \tag{50}$$

The second derivative of  $P_R(V_m)$  with respect to  $Y$  is positive everywhere and thus,  $P_R(V_m)$  is an upward concave function of  $Y$ , and of  $E$ . Since the first derivative has a zero on the positive  $Y$ -axis,  $P_R(V_m)$  is minimum at this point. It may then meet  $P_{Amax}(V_m)$  at most at two values of  $E$ , with  $P_R(V_m) \leq P_{Amax}(V_m)$  for all  $E$  between these two values. Fig. 11(b) shows the curves of  $P_R(V_m)$  and  $P_{Amax}(V_m)$  as a function of  $E$ . This graph indicates that  $P_R(V_m) \leq P_{Amax}(V_m)$  is satisfied for all values of  $E$  between 500 and 1700 m<sup>2</sup>/s<sup>2</sup>. The fact that  $P_R$  is also below  $P_{Amax}$  at  $V_M$  indicates that trajectories with  $\theta_H=10^\circ$  and  $R=100$  m are flyable by the Cessna 182 for all values of  $E \in [500, 1700]$  m<sup>2</sup>/s<sup>2</sup>.

Fig. 12 shows the equivalent data for the Silver Fox, on a trajectory with  $\theta_H=50^\circ$  and  $R=40$  m. In Fig. 12(a) are the curves of  $P_R(V_M)$  and  $P_A(V_M)$  as a function of  $E$ . It can be seen on this graph that  $P_R(V_M) \leq P_{Amax}(V_M)$  is satisfied for all values of  $E$  between 651 and 706 m<sup>2</sup>/s<sup>2</sup>. Fig. 12(b) shows

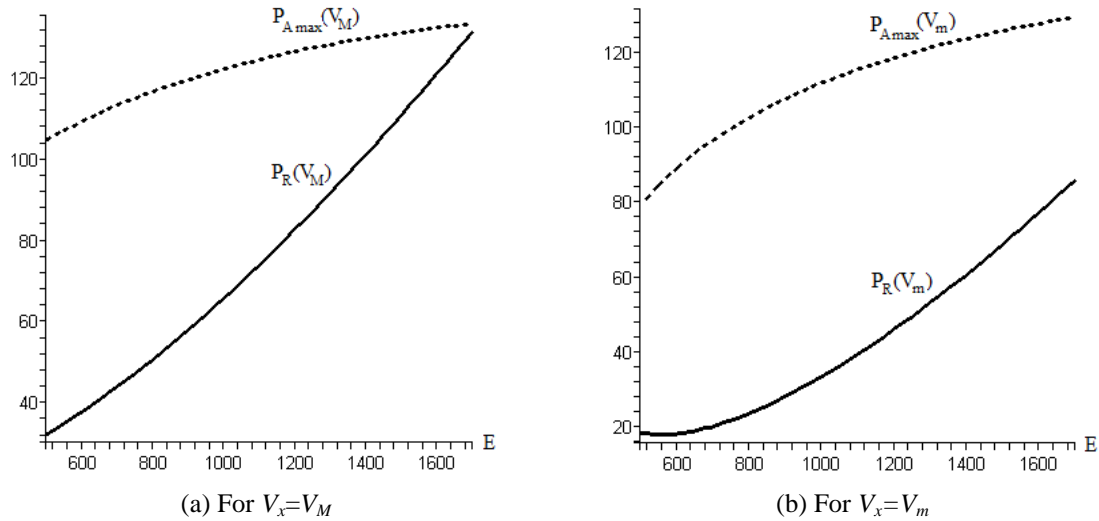


Fig. 11  $P_R(V_x)$  in full line, and  $P_{Amax}(V_x)$  in dotted line, as a functions of  $E$ , for the Cessna 182, when  $E$  varies from 500 to 1700  $m^2/s^2$ , and the value of  $P_R$  and  $P_{Amax}$  have been divided by 1000

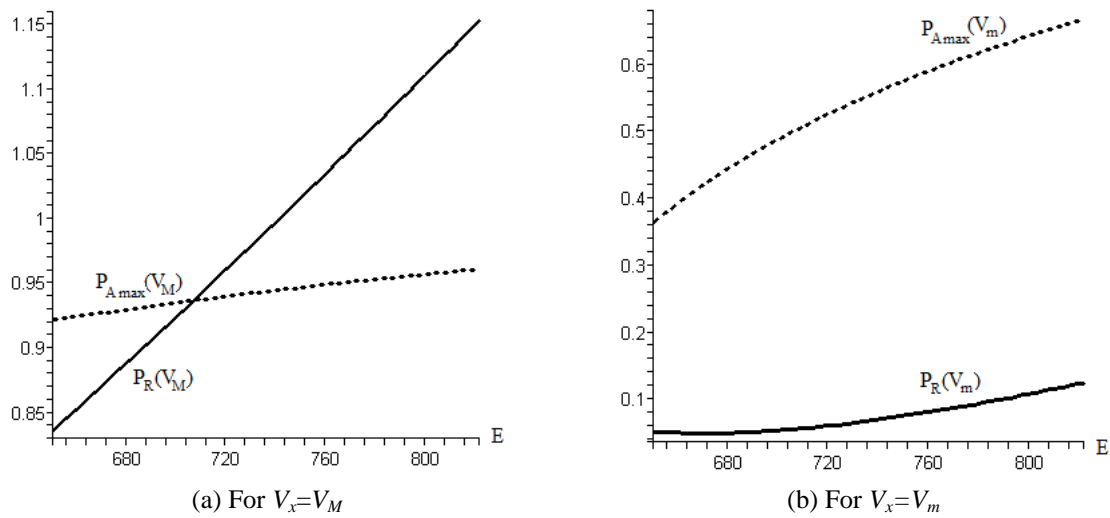


Fig. 12  $P_R(V_x)$  in full line, and  $P_{Amax}(V_x)$  in dotted line, as a functions of  $E$ , for the Silver Fox, when  $E$  varies from 650 to 820  $m^2/s^2$ , and the value of  $P_R$  and  $P_{Amax}$  have been divided by 1000

that  $P_R(V_M) \leq P_{Amax}(V_M)$  everywhere in that range of  $E$ . Therefore, the Silver Fox can fly this trajectory for all  $E \in [651, 706] m^2/s^2$ .

### 8. Thrust required for jet airplanes

For jet airplanes, the maximum thrust available can be considered to be independent of the speed  $V_\infty$ . Therefore, the power sufficiency constraint can be stated as the inequality  $T_R \leq T_{Amax}$ , in

which  $T_R$  is the thrust required along the trajectory and  $T_{Amax}$  is the maximum thrust that the engine can provide. Eq. (4) gives the thrust required as

$$T_R = D = \frac{1}{2} \rho_\infty S C_D V_\infty^2 = \frac{1}{2} \rho_\infty S \left[ C_{D0} + \frac{C_L^2}{\pi e A R} \right] V_\infty^2. \quad (51)$$

When  $C_L$  is replaced by its value from Eq. (3.21), one obtains

$$T_R = C V_\infty^2 - 3 \Gamma [E - gZ] + \Gamma A V_\infty^{-2} \quad (52)$$

in which the parameters  $C$ ,  $\Gamma$  and  $A$  are the same ones as defined in Eqs. (42), (43) and (7.8). The constraint  $T_R \leq T_{Amax}$  yields the following inequality

$$G(V_\infty^2) \leq 0$$

with

$$G(U) = C U^2 - [3 \Gamma (E - gZ) + T_{Amax}] U + \Gamma A. \quad (53)$$

The function  $G$  is quadratic and corresponds to a parabola that is concave upward. Thus, Ineq. (53) will hold for all  $V_\infty \in [V_m, V_M]$  if and only if it holds at both points  $V_m$  and  $V_M$ . Fig. 13(a) shows the thrust required  $T_R$  and the maximum thrust available  $T_{Amax}$  as functions of the speed  $V_\infty$  for the F-16 on a circular trajectory inclined with  $\theta_H = 85^\circ$ ,  $R = 400$  m and  $E = 10\,000$  m<sup>2</sup>/s<sup>2</sup>. It is clear from this graph that  $T_R \leq T_{Amax}$  at both  $V_m$  and  $V_M$ .

### 8.1 Condition at $V_M$

At  $V_M$ , Ineq. (53) becomes

$$4(\bar{C}_{D0} + \Gamma) E^2 + 2[2\Gamma gZ - T_{Amax}] E + \Gamma g^2 R^2 \leq 0. \quad (54)$$

We note that the second term on the LHS must be negative because all the other terms are positive. The quadratic expression in  $E$ , on the LHS, corresponds to a parabola that is concave upward. In Fig. 13(b), the full line represents  $T_R(V_M)$  and the dotted line  $T_{Amax}(V_M)$ , as a functions of  $E$  that varies from 8 650 to 13 200 m<sup>2</sup>/s<sup>2</sup> for the F-16. Ineq. (54) can hold only if the quadratic function on the LHS of this inequality has real roots, that is, if its discriminant  $\Delta_1$  is positive, with

$$\Delta_1 = 4[T_{Amax} - 2\Gamma gZ]^2 - 16(\bar{C}_{D0} + \Gamma)\Gamma g^2 R^2 \geq 0. \quad (55)$$

Ineq. (55) can be seen to be equivalent to

$$\cos(\theta) \leq \frac{T_{Amax}}{2\Gamma gR} - \sqrt{\frac{\bar{C}_{D0} + \Gamma}{\Gamma}}. \quad (56)$$

Because  $\cos(\theta)$  must be non-negative, Ineq. (56) implies that

$$T_{Amax} > 2\sqrt{\gamma \bar{C}_{D0}} \quad (57)$$

and

$$R \geq \frac{2\gamma}{g\sqrt{T_{Amax}^2 - 4\gamma \bar{C}_{D0}}}. \quad (58)$$

Ineq. (54) is then satisfied either if and only if

$$r_- \leq E \leq r_+$$

with

$$r_{\pm} = \frac{I}{8(\bar{C}_{D0} + \Gamma)} \left\{ 2 [T_{Amax} - 2\Gamma g Z] \pm \sqrt{\Delta_1} \right\}. \tag{59}$$

### 8.2 Condition at $V_m$

At  $V_m$ , Ineq. (53) becomes

$$4(\bar{C}_{D0} + \Gamma)E^2 - 2[2(4\bar{C}_{D0} + 5\Gamma)gZ + T_{Amax}]E + [8(2\bar{C}_{D0} + 3\Gamma)g^2Z^2 + 4T_{Amax}gZ + \Gamma g^2R^2] \leq 0 \tag{60}$$

Since the LHS of Ineq. (60) corresponds to an upward concave parabola that has its minimum at a point on the positive axis and a positive intercept on the vertical axis. It must have two real roots for Ineq. (60) to be possible. Its discriminant is  $\Delta_2$

$$\Delta_2 = 4[T_{Amax} + 2\Gamma g Z]^2 - 16(\bar{C}_{D0} + \Gamma)\Gamma g^2 R^2 \geq 0. \tag{61}$$

Ineq. (55) implies that  $\Delta_2$  is always positive. Ineq. (60) will then be satisfied if and only if

$$s_- \leq E \leq s_+$$

with

$$s_{\pm} = \frac{I}{8(\bar{C}_{D0} + \Gamma)} \left\{ 2 [T_{Amax} + 2(4\bar{C}_{D0} + 5\Gamma)gZ] \pm \sqrt{\Delta_2} \right\}. \tag{62}$$

In Fig. 13(c), the full line represents  $T_R(V_m)$  and the dotted line  $T_{Amax}(V_m)$ , as functions of  $E$  that varies from 8 650 to 13 200  $m^2/s^2$  for the F-16.

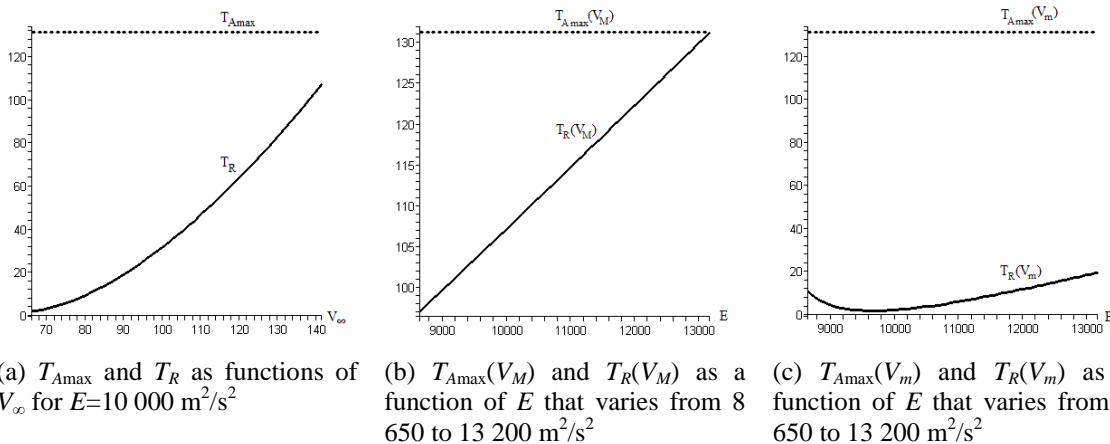


Fig. 13 Maximum thrust available  $T_{Amax}$  (dotted line) and thrust required  $T_R$  (full line) for the F-16 on a trajectory with  $\theta_H=85^\circ$ ,  $R=400$  m.  $T_R$  and  $T_{Amax}$  have been divided by 1000

## 9. Flyability analysis

We have obtained conditions for the flyability of inclined low thrust circular trajectories. We are not able to solve all of them together and obtain definite ranges of parameters that are suitable for a particular airplane. Nevertheless, it is straightforward to use our results to devise a procedure for testing whether trajectories are flyable or not. We describe this procedure below and show how it can be used to produce tables of parameters for flyable trajectories. In this discussion, we found it more natural to use the angle of inclination with the horizontal plane  $\theta_H$  as variable instead of that with the  $z$ -axis  $\theta$ . Note that the only parameters required to completely specify a circular low thrust trajectory are the angle of inclination  $\theta$  (or  $\theta_H$ ) the radius  $R$  and the “energy”  $E$ . Once these are known, all the details of the trajectory can be computed.

### 9.1 Procedure for propeller driven airplanes

1. Use Ineq. (27), which pertains to the bounds on the load factor, to compute the upper bound  $\theta_{H\max\_1}$  on the inclination angle  $\theta_H$ .
2. Select an angle of inclination  $\theta_H$  such that  $\theta_H < \theta_{H\max\_1}$ .
3. Use Ineq. (34), which pertains to the bounds on the lift coefficient, to compute a lower bound  $R_{\min\_1}$  on the radius of the trajectory.
4. Select a radius  $R$  such that  $R \geq R_{\min\_1}$ .
5. Use Ineq. (26), which pertains to the bounds on the load factor, to compute the upper bound  $E_{\max\_1}$  on the energy  $E$ .
6. Use Ineqs. (35) and (36), which pertain to the bounds on the lift coefficient, to compute the lower bounds  $E_{\min\_1}$  and  $E_{\min\_2}$ .
7. Compute the overall bound  $E_{\min} = \max\{E_{\min\_1}, E_{\min\_2}\}$

The following part of the procedure is to ensure that  $P_R \leq P_{A\max}$ .

1. Consider the values of  $P_R(V_M)$  and  $P_{A\max}(V_M)$  given in Eqs. (39) and (49), for  $E \in [E_{\min}, E_{\max\_1}]$ . Either with the help of the graph of these two functions or some numerical method, determine the range of  $E$  for which  $P_R(V_M) \leq P_{A\max}(V_M)$ .
2. Perform the same procedure as in step 8 for  $P_R(V_m)$  and  $P_{A\max}(V_m)$  given in Eqs. (39) and (50) and determine the range of  $E$  for which  $P_R(V_m) \leq P_{A\max}(V_m)$ .
3. Compute the range of allowed values of  $E$  as the intersection of the above computed two ranges. If this intersection is empty, then the selected inclination angle  $\theta_H$  and radius  $R$  do not correspond to a flyable trajectory.

By performing successively the above procedure with various values of  $\theta_H$  and  $R$ , one can produce a table of allowed parameters for which a particular airplane can fly the low thrust circular trajectories. We will show an example of this procedure in Section 11.

### 9.2 Procedure for jet airplanes

1. Verify that Ineq. (57) holds, without which the airplane cannot fly any circular trajectory.
2. Perform Step 1 of Section 10.2 to obtain  $\theta_{H\max\_1}$ .
3. Use Ineq. (56), which pertains to the bound on the thrust, to obtain the upper bound  $\theta_{H\max\_2}$  on the inclination angle  $\theta_H$ .
4. Select an angle  $\theta_H$  that satisfies  $\theta_H < \theta_{H\max\_1}$  and  $\theta_H \leq \theta_{H\max\_2}$ .

5. Perform Step 3 of Section 10.2 to obtain  $R_{\min_1}$ .
6. Use Ineq. (58), which pertains to the bound on the thrust, to obtain the lower bound on  $R$ :  $R_{\min_2}$ .
7. Select a radius  $R$  such that  $R \geq R_{\min}$  with  $R_{\min} = \max\{R_{\min_1}, R_{\min_2}\}$ .
8. Perform Steps 5 and 6 of Section 10.2 to obtain  $E_{\max_1}$ ,  $E_{\min_1}$  and  $E_{\min_2}$ .
9. Use Eq. (59), which pertains to the bound on the thrust, to obtain the lower and upper bounds:  $E_{\min_3}$  and  $E_{\max_2}$ .
10. Use Eq. (62), which pertains to the bound on the thrust, to obtain the lower and upper bounds:  $E_{\min_4}$  and  $E_{\max_3}$ .
11. Compute the overall bounds  $E_{\min} = \max\{E_{\min_1}, E_{\min_2}, E_{\min_3}, E_{\min_4}\}$  and  $E_{\max} = \min\{E_{\max_1}, E_{\max_2}, E_{\max_3}\}$

For the selected inclination angle  $\theta_H$  and radius  $R$  the range of allowed values of  $E$  is  $[E_{\min}, E_{\max}]$ . If this range is empty, then the selected inclination angle  $\theta_H$  and radius  $R$  do not correspond to a flyable trajectory. If it is not empty, then all  $E$ 's in this range are allowed.

For jet airplanes, the necessary and sufficient conditions for trajectories to be flyable have been solved completely. Thus, the above computations could be performed quickly on-board the airplane, in order to determine if a considered trajectory is flyable or not. Nevertheless, in order to give an idea of the possible performances of the *F-16*, we calculated tables as for the above propeller airplanes.

## 10. Examples of computation

In this section, we illustrate the procedure described in Section 10, to determine what low thrust circular trajectories a particular airplane can fly. We do so for the three different types of airplanes.

### 10.1 Cessna 182 Skylane

The bounds  $\theta_{H\max_1}$  and  $R_{\min_1}$  are independent of the other parameters. Thus, their values hold for all low thrust circular trajectories. Their values are

$$\theta_{H\max_1} = 48.45^\circ \text{ and } R_{\min_1} = 37.11 \text{ m.}$$

Flyability tables could be produced for each value of  $\theta_H$ , starting with  $0^\circ$  and increasing the angle by some fixed increment, until the upper  $\theta_{H\max_1}$  is reached. These tables can be constructed as follows.

1. For each value of  $\theta_H$ , consider successively increasing values of  $R$ , from  $R_{\min_1}$  until a radius is reached after which no trajectory is flyable.  $R$  could be increased by a fixed increment, such as 25 m, as we do here.
2. For each selected  $\theta_H$  and  $R$ , compute the range of possible values of  $E \in [E_{\min}, E_{\max}]$  for which all the constraints are satisfied.

Tables 1-3 are examples of tables of parameters obtained at various  $\theta_H$ . The smallest and the largest radius in the table respectively correspond to the first one and the last one at which the trajectory is flyable.

Similar flyability tables for flights at constant speeds on inclined circular trajectories have been produced in Labonté (2015b). The comparison between these tables and those produced here

Table 1 Flyability table for  $\theta_H=10^\circ$

		$\theta_H=10^\circ$										
$R$	50	75	100	125	150	175	200	225	250	275	...	800
$E_{\min}$	394	445	523	606	690	775	860	945	1030	1115	...	2903
$E_{\max}$	803	1285	1713	2012	2224	2378	2491	2576	2641	2693	...	2947

Table 2 Flyability table for  $\theta_H=30^\circ$

		$\theta_H=30^\circ$						
$R$	50	75	100	125	150	175	200	
$E_{\min}$	650	893	1141	1388	1635	1882	2128	
$E_{\max}$	700	1176	1568	1896	2115	2277	2398	

Table 3 Flyability table for  $\theta_H=40^\circ$

		$\theta_H=40^\circ$			
$R$	75	100	125	150	
$E_{\min}$	1091	1412	1731	2049	
$E_{\max}$	1131	1508	1845	2068	

clearly shows the advantages of flying at low thrust. We did not find it worthwhile reproducing completely the latter tables here for comparison purposes; however, an evident advantage of flying at low thrust is that the maximum angle of inclination  $\theta_H$  for trajectories at constant speeds is only  $10^\circ$  while at low thrust, it is  $40^\circ$  (note that there are some errors in the tables in Labonté (2015b); so that actually the flights at  $15^\circ$  are not possible).

### 10.2 Silver Fox like UAV

For this airplane, the bounds  $\theta_{H\max\_1}$  and  $R_{\min\_1}$  are  $\theta_{H\max\_1}=90^\circ$  and  $R_{\min\_1}=12.50$  m.

The tables of parameters are constructed exactly as for the Cessna 182. Tables 4-6 are examples of tables of parameters obtained at various  $\theta_H$ . The entries in the tables correspond to values of  $R$  at each 10 m. The smallest and the largest radius in the table respectively correspond to the first one and the last one at which the trajectory is flyable.

Comparison of these tables with those shown in Labonté (2015b) for flights at constant speed, clearly show the advantage of flying at low thrust. Indeed, for flights at constant speeds, the maximum angle of inclination  $\theta_H$  is only  $10^\circ$ , while at low thrust, it is  $60^\circ$ .

### 10.3 F16 Fighting Falcon

For this airplane, the bounds  $\theta_{H\max\_1}$  and  $R_{\min\_1}$  are

$$\theta_{H\max\_1}=90^\circ, R_{\min\_1}=299,67 \text{ m and } R_{\min\_1}= 82.49 \text{ m.}$$

The flyability tables are constructed as described in Section 10.2. Tables 7-9 are examples of flyability tables for various values of  $\theta_H$ . The entries in the tables correspond to values of  $R$  at each

Table 4 Flyability table for  $\theta_H=15^\circ$ 

		$\theta_H = 15^\circ$										
$R$	15	25	35	45	55	65	75	85	95	105	...	165
$E_{\min}$	162	188	237	288	338	389	440	491	542	593	...	898
$E_{\max}$	339	569	701	776	821	850	869	883	893	900	...	921

Table 5 Flyability table for  $\theta_H=35^\circ$ 

		$\theta_H=35^\circ$				
$R$	15	25	35	45	55	65
$E_{\min}$	242	332	446	560	673	787
$E_{\max}$	311	534	676	755	803	834

Table 6 Flyability table for  $\theta_H=60^\circ$ 

		$\theta_H=60^\circ$	
$R$	25	35	
$E_{\min}$	468	642	
$E_{\max}$	503	653	

Table 7 Flyability table for  $\theta_H=30^\circ$ 

		$\theta_H=30^\circ$							
$R$	350	450	550	650	750	850	950	1050	...
$E_{\min}$	6046	5687	6662	7650	8640	9631	10621	11611	...
$E_{\max}$	11488	18618	22795	26940	31084	35229	39373	43518	...

100 m, starting the first radius at which the trajectory is flyable.

We note that the parameters determined for very large radii trajectories are not as accurate as those for smaller radii. Indeed, the derivation of our formulas assumed that the difference in air density could be neglected along the trajectory. However, with large radii, the difference of altitude between the lowest and the highest points of the trajectory is also large. There is then an appreciable difference in the thrust available and the thrust required to fly the trajectory. For example, as described in Example 6.4 of Anderson (2000), in the first order approximation the thrust available depends on the altitude as  $T_A(h) = \frac{\rho_\infty(h)}{\rho_\infty(0)} T_A(0)$ . For the *F-16*, the thrust available

at sea level is 131 222N. For the trajectory at  $30^\circ$  with radius  $R=1050$  m the decrease in thrust available  $T_A$  is 12 690N between the lowest and the highest points. At  $60^\circ$ , for  $R=1050$  m, it is 21 373 N and at  $90^\circ$  with  $R=1075$ , it is 24 956 N. Nevertheless, one should remember that the object of the present study is circular trajectories to be used for connecting rectilinear segments of trajectories. Thus, they would not be very large radius circular trajectories; in the connections, the circular arcs will rather be desired to be as short as possible. We have included such large radii trajectories in our tables only to show the way the trajectory parameters change in relation to each other, according to the formulas we have obtained. Note that larger radii as those appearing in the tables are possible.

Table 8 Flyability table for  $\theta_H=60^\circ$

	$\theta_H = 60^\circ$								
$R$	350	450	550	650	750	850	950	1050	...
$E_{\min}$	9051	8605	10360	12103	13838	15567	17290	19010	...
$E_{\max}$	10319	17212	21884	25862	29841	33820	37799	41778	...

Table 9 Flyability table for  $\theta_H=90^\circ$

	$\theta_H = 90^\circ$								
$R$	375	475	575	675	775	875	975	1075	...
$E_{\min}$	8166	10230	12235	12247	16249	18244	20233	22218	...
$E_{\max}$	11482	18557	22540	26460	30380	34300	38220	42140	...

Again, the comparison of these tables with those shown in Labonté (2015b) for flights at constant speeds, show an evident advantage of flying at low thrust. For flights at constant speed, the maximum angle of inclination  $\theta_H$  is only  $40^\circ$ , while at low thrust, it is up to  $90^\circ$ .

## 10. Conclusions

We have defined a particular way for an airplane to fly on an inclined circular trajectory, such that all the components of the required thrust cancel out, except for the drag. Such a motion is then near optimal in terms of power requirements. The airplane moves on such trajectories essentially as a rigid pendulum on which a drag force is acting. To our knowledge, this type of airplane motion had not been studied before.

We have solved the equations of motion and obtained explicit expressions for the position, the velocity, the angle of bank, the load factor, the lift coefficient and the thrust or power required. We have determined the limits on the trajectory parameters, i.e. the angle of inclination, the radius and the speed, that follow from the limits on the airplane characteristic parameters. The formulas we have obtained are exact in so far as the rotational motions of the airplane can be considered as not affecting the motion of its center of mass, and the air density can be considered constant on the trajectory. They yield necessary and sufficient conditions for an airplane to be able to fly on such trajectories. They are original formulas that apply to all airplanes. As such, they constitute a valuable tool for the analysis of airplane performance and mission planning.

They are simple enough that trajectories can be analyzed in real time on board any airplane. The computations could even be performed with a microcontroller on board a small UAV.

We have illustrated the application of these formulas to airplanes with a reciprocating engine and a constant speed propeller or with a fixed pitch propeller, and airplanes with jet propulsion. We have described a procedure for testing the flyability of specific trajectories and for constructing tables of flyable trajectory parameters. The airplanes considered in our sample calculations are representative of a wide range of airplanes. They are similar to the Cessna 182 Skylane, the Silver Fox UAV and the F-16 Fighting Falcon jet. These are the same three airplanes used in Labonté (2015b), for the flyability study of inclined circular trajectories flown at constant speed. It was thus straightforward to compare the flyabilities of our low thrust trajectories with those flown at

constant speeds. It was seen that the same airplanes can fly much more inclined low thrust circular trajectories than constant speed circular trajectories.

## References

- Aeronautics Learning Laboratory for Science Technology and Research (ALLSTAR) of the Florida International University, (2011), Propeller Aircraft Performance and The Bootstrap Approach, Miami, FL, USA, <http://www.allstar.fiu.edu/aero/BA-Background.htm>.
- Airliners.net (2015), Santa Monica, CA, USA, <http://www.airliners.net/aircraft-data/stats.main?id=145>
- Ambrosino, G., Ariola, M., Ciniglio, U., Corraro, F., De Lellis, E. and Pironti, A. (2009), "Path generation and tracking in 3-D for UAVs", *IEEE Tran. Control Syst. Technol.*, **17**(4), 980-988.
- Anderson, E.P. (2002), "Extremal control and unmanned air vehicle trajectory generation", MSc Dissertation, Brigham Young University, Utah, USA.
- Anderson, E.P., Beard, R.W. and McLain, T.W. (2005), "Real-Time dynamic trajectory smoothing for unmanned air vehicles", *IEEE Tran. Control Syst. Technol.*, **13**(3), 471-477.
- Anderson, J.D. Jr. (2000), *Introduction to Flight*, Fourth Edition, McGraw-Hill Series in Aeronautical and Aerospace Engineering, Toronto, Ontario, Canada.
- Babaei, A.R. and Mortazavi, M. (2010), "Three-dimensional curvature-constrained trajectory planning based on in-flight waypoints", *J. Aircraft*, **47**(4), 1391-1398.
- Bottasso, C.L., Leonello, D. and Savini, B. (2008) "Path planning for autonomous vehicles by trajectory smoothing using motion primitives", *IEEE Tran. Control Syst. Technol.*, **16**(6), 1152-1168.
- Cavcar, M. (2004), Propeller, Anadolu University, School of Civil Aviation, Eskisehir, Turkey. <http://home.anadolu.edu.tr/~mcavcar/common/Propeller.pdf>
- Chandler, P., Rasmussen, S. and Pachter, M. (2000), "UAV cooperative path planning", *Proceedings of the AIAA Guidance, Navigation, and Control Conference*, Denver, Colorado, USA, August.
- Chitsaz, H. and LaValle, S.M. (2007), "Time-optimal paths for a Dubins airplane", *Proceedings of the 46th IEEE Conference on Decision and Control*, New Orleans, LA, USA, December.
- Cowley, W.L. and Levy, H. (1920), *Aeronautics Theory and Experiment*, 2nd Edition, Edward Arnold, London, England.
- Currawong Engineering (2016), UAV Engines, Kingston, Australia. [http://www.currawongeng.com/products/uav\\_engines/](http://www.currawongeng.com/products/uav_engines/)
- Dubins, L.E. (1957), "On curves of minimal length with a constraint on average curvature and with prescribed initial and terminal positions and tangents", *Am. J. Math.*, **79**, 497-516.
- Faculty of Engineering, University of Porto (2013), SilverFox Block B-3 Specifications, Porto, Portugal. [http://whale.fe.up.pt/asaf/images/f/f8/UAV\\_SF\\_Specs.pdf](http://whale.fe.up.pt/asaf/images/f/f8/UAV_SF_Specs.pdf)
- Filippone, A. (2000), "Data and performances of selected aircraft and rotorcraft", *Prog. Aerospace Sci.*, **36**, 629-654.
- Gradshteyn, I.S. and Ryzhik, I.M. (1965), *Table of Integrals Series and Products*, Academic Press, New York, NY, USA.
- Hota, S. and Ghose, D. (2010), "Optimal geometrical path in 3D with curvature constraint", *Proceedings of the IEEE/RSJ International Conference on Intelligent Robots and Systems (IROS)*, Taipei, Taiwan, October.
- Hwangbo, M., Kuffner, J. and Kanade, T. (2007), "Efficient two-phase 3D motion planning for small fixed-wing UAVs", *Proceedings of the IEEE International Conference on Robotics and Automation*, Rome, Italy, April.
- Jeyaraman, S., Tsourdos, A., Zbikowski, R. and White, B. (2005), "Formal techniques for the modelling and validation of a co-operating UAV team that uses Dubins set for path planning", *Proceedings of the 2005 American Control Conference*, Portland, OR, USA, June.
- Jia, D. and Vagners, J. (2004), "Parallel evolutionary algorithms for UAV path planning", *Proceedings of the*

- AIAA 1st Intelligent Systems Technical Conference, Chicago, IL, September.
- Judd, K.B. (2001), "Trajectory planning strategies for unmanned air vehicles", MSc Dissertation, Brigham Young University, Utah, USA.
- Jun, M. and D'Andrea, R (2003), *Path Planning for Unmanned Aerial Vehicles in Uncertain and Adversarial Environments*, Chapter 6, "Cooperative control: models, applications and algorithms", Eds. Butenko, S., Murphey, R. and Pardalos, P., Kluwer Academic Publishers, Norwell, MA, USA.
- Korkan, K.D., Gregorek, G.M. and Mikkelson, D.C. (1980), "A theoretical and experimental investigation of propeller performance methodologies", *Proceedings of the AIAA-80-1240, AIAA / SAE / ASME 16th Joint Propulsion Conference*, Hartford, CT, USA, June.
- Labonté, G. (2011), "Formulas for the fuel of climbing propeller driven planes", *Aircraft Eng. Aerosp. Tech.*, **84**(1), 23-36.
- Labonté, G. (2015a), "Simple formulas for the fuel of climbing propeller driven airplanes", *Adv. Aircraft Spacecraft Sci.*, **2**(4), 367-389.
- Labonté, G. (2015b), "Airplanes at constant speeds on inclined circular trajectories", *Adv. Aircraft Spacecraft Sci.*, **3**(4), 399-425.
- Li, X., Xie, J., Cai, M., Xie, M. and Wang, Z. (2009), "Path planning for UAV based on improved A\* algorithm", *Proceedings of the 9th International Conference on Electronic Measurement & Instruments, ICEMI '09*, Beijing, China, August.
- Lin, Y. and Saripalli, S. (2014), "Path planning using 3D Dubins curve for unmanned aerial vehicles", *Proceedings of the 2014 International Conference on Unmanned Aircraft Systems (ICUAS)*, Orlando, FL, USA, May.
- Lockheed-Martin (2015), F-16 Specifications, Bethesda, MD, USA, <http://lockheedmartin.com/us/products/f16/F-16Specifications.html>
- Lugo-Cardenas, I., Flores, G., Salazar, S. and Lozano, R. (2014), "Dubins path generation for a fixed wing UAV", *Proceedings of the 2014 International Conference on Unmanned Aircraft Systems (ICUAS)*, Orlando, FL, USA, May.
- Mair, W.A. and Birdsall, D.L. (1992), *Aircraft Performance*, Cambridge Aerospace Series 5, Cambridge University Press, Cambridge, GB.
- Marion, J.B. (1970), *Classical Dynamics of Particles and Systems*, 2nd Edition, Academic Press, New York, NY, USA.
- McIver, J. (2003), Cessna Skyhawk II /100, Performance Assessment, Temporal Images, Melbourne, Australia. <http://www.temporal.com.au/c172.pdf>
- Phillips, W.F. (2004), *Mechanics of Flight*, John Wiley & Sons, Inc., Hoboken, New Jersey, USA
- Rathbun, D., Kragelund, S., Pongpunwattan, A. and Capozzi, B. (2002), "An evolution based path planning algorithm for autonomous motion of a UAV through uncertain environments", *Proceedings of the 21st Digital Avionics Systems Conference*, 8D2-1-8D2-12, Irvine, CA, USA, October.
- Roud, O. and Bruckert D. (2006), Cessna 182 Training Manual, Red Sky Ventures and Memel CATS, Second Edition 2011, Windhoek, Namibia.
- Sadraey, M. (2009), *Aircraft Performance Analysis*, VDM Verlag Dr. Müller, Saarbrücken, Germany.
- Shanmugavel, M., Tsourdos, A. and White, B.A. (2010), "Collision avoidance and path planning of multiple UAVs using flyable paths in 3D", *Proceedings of the 15th International Conference on Methods and Models in Automation and Robotics (MMAR)*, Miedzydroje, Poland, August.
- Singh, S. and Padhi, R. (2009), "Automatic path planning and control design for autonomous landing of UAVs using dynamic inversion", *Proceedings of the 2009 American Control Conference*, St. Louis, MO, USA, June.
- Stengel, R.F. (2004), *Flight Dynamics*, Princeton University Press, Princeton, NJ, USA.
- Torroella, J.C. (2004) "Long range evolution-based path planning for UAVs through realistic weather environments", MSc Dissertation, University of Washington, Washington, USA.
- Von Mises, R. (1945), *Theory of Flight*, Dover Publications Inc., New York, NY, USA.
- Wang Zhong and Li Yan (2014), "A target visiting path planning algorithm for the fixed-wing UAV in obstacle environment", *Proceedings of the 2014 IEEE Chinese Guidance, Navigation and Control*

Conference (CGNCC), Yantai, China, August.

Yang, K. and Sukkariéh, S. (2010), “An analytical continuous-curvature path-smoothing algorithm”, *IEEE Tran. Robot.*, **26**(3), 561-568.

Zheng, C., Ding, M. and Zhou, C. (2003), “Real-Time route planning for unmanned air vehicle with an evolutionary algorithm”, *Int. J. Patt. Recog. Artif. Intel.*, **17**(1), 63-81.

EC

## Nomenclature

$AR$  = aspect ratio =  $b^2/S$

$b$  = wingspan

$\beta$  = bank angle

$C_D$  = global drag coefficient for the airplane =  $C_{D0} + \frac{C_L^2}{\pi e AR}$  (Drag polar)

$C_{D0}$  = global drag coefficient at zero lift

$C_L$  = global lift coefficient for airplane

$C_{Lmax}$  = maximum value of  $C_L$

$D$  = drag =  $\frac{1}{2} \rho_\infty S C_D V_\infty^2$

$e$  = Oswald's efficiency factor

$g$  = gravitational constant =  $9.8 \text{ m/s}^2$

$L$  = lift =  $\frac{1}{2} \rho_\infty S C_L V_\infty^2$

$n_{max}$  = maximum value of load factor

$n_{min}$  = minimum value of load factor

$P$  = power of the engine in Watt

$P_{Amax}$  = maximum power available for propulsion

$P_R$  = power required for a certain motion

$S$  = wing area

$t$  = time

$T$  = thrust of an engine

$T_{Amax}$  = maximum thrust available

$T_R$  = thrust required for a certain motion

$V_\infty$  = airplane speed with respect to the undisturbed air in front of it

$V_{min}$  = minimum value of  $V_\infty$

$V_{max}$  = maximum value of  $V_\infty$

$W$  = weight of airplane

$W_1$  = weight of empty airplane

$W_0$  = maximum total weight of airplane at take off

$\eta$  = propeller efficiency

$\rho_s$  = air density at sea level =  $1.225 \text{ kg/m}^3$

$\rho_\infty$  = density of undisturbed air in front of airplane

## Appendix A: Reference airplanes

### A.1 Cessna 182 skylane

The characteristic parameters for the Cessna 182 can be found in Airliners.net (2015), Roud and Bruckert (2006), McIver (2003). Some of the parameters, which were not readily available, were estimated from those of the very similar Cessna 172.

Table 10 Characteristic parameters of the Cessna 182 Skylane

$W_1=7,562.0$ N	$W_0=11,120.6$ N	
$b=11.02$ m	$S=16.1653$ m <sup>2</sup>	$e=0.75$
$C_{Lmax}=2.10$	$C_{D0}=0.029$	$n_{max}=3.8, n_{min}=-1.52$
$P_{Amax}=171.511$ kW, 2,600 rpm, at sea level		
Propeller: constant speed, diameter=2.08 m, $\eta_{max}=0.80$		

### A.2 Silver fox like UAV

The Silver Fox UAV is presently produced by Raytheon. Some of its specifications can be found at the Faculty of Engineering, University of Porto (2013). It has an off-the-shelf Radio Controlled plane engine that is described at the Currawong Engineering website (2016). Some of the parameters given below were estimated by comparison with similar small UAVs.

Table 11 Characteristic parameters of a Silver Fox like UAV

$W_1=72.35$ N	$W_0=119.6$ N	
$b=2.4$ m	$S=0.768$ m <sup>2</sup>	$e=0.8$
$C_{Lmax}=1.26$	$C_{D0}=0.0251$	$n_{max}=5.0, n_{min}=-2.0$
$P_{Amax}=1,491$ W at 7,500 rpm, at sea level		
Propeller: fixed speed, diameter=0.56 m, $\eta_{max}=0.83$		

### A.3 F16 fighting falcon

The General Dynamics/Lockheed Martin F-16 Fighting Falcon is a single-engine fighter aircraft originally developed for the United States Air Force. Its characteristic parameters can be found in Lockheed-Martin (2015), Filippone (2000), Sadraey (2009). The maximum value of the lift coefficient and the maximum negative load factor were estimated from those of other fighter airplanes.

Table 12 Characteristic parameters of an F16 like jet

$W_1=90,237.4$ N	$W_0=213,365.6$ N	
$b=10.0$ m	$S=27.87$ m <sup>2</sup>	$e=0.8$
$C_{Lmax}=1.8$	$C_{D0}=0.026$	$n_{max}=9.0, n_{min}=-3$
$T_{Amax}=131,222.5$ N		